NURBS Warps

Florent Brunet[123]
florent.brunet@univ-bpclermont.fr
Adrien Bartoli[1]
adrien.bartoli@gmail.com
Nassir Navab[2]
navab@cs.tum.edu
Rémy Malgouyres[3]
remy.malgouyres@laic.u-clermont1.fr

[1] LASMEA
CNRS/Université Blaise Pascal
Clermont-Ferrand, France
[2] CAMPAR
Technische Universität München
Garching bei München, Germany
[3] LAIC
Université d'Auvergne
Clermont-Ferrand, France

Abstract

Standard Free-Form Deformations (FFD) built upon tensor-product B-Splines have been proved useful to model the warp between two views of a deformable surface. In this paper, we show that the standard FFD is the affine projection of a threedimensional tensor-product B-Spline surface. We construct a new tensor-product warp relying on Non-Uniform Cubic B-Spline: the NURBS-Warp. We show that this new warp is an extension of the standard FFD that describes the perspective camera model. We propose algorithms that compute the parameters of a NURBS-Warp from point correspondences. Our NURBS-Warp is compared to the standard FFD warp for both synthetic and real images. These experiments show that our NURBS-Warp gives better results than the other warps, especially when the perspective effects are important.

1 Introduction

Given two images of a threedimensional surface, a warp is an $\mathbb{R}^2 \rightarrow \mathbb{R}^2$ function that maps a point from the first image to the corresponding point in the second image (see figure 1). For example, two images of a rigid scene taken by a perspective camera that rotates around its optical center are related to each other by an homographic warp. In the presence of deformable surfaces, and for an arbitrary camera displacement, the warp has to be more complex. Several parametric warps were proposed and proved efficient, such as the Thin-Plate Spline warp [4] and the B-Spline warp (hereinafter abbreviated *BS-Warp* and also called Free-Form Deformation [10]).

A parametric warp is a function model. It depends on a set of parameters in a vector $\mathbf{x}$. For instance, these parameters can be the weights of a Thin-Plate Spline or the coefficients of an homography matrix. Estimating a warp consists in finding the value of the parameter vector that minimizes some criterion. There exists two classes of approaches. In the feature-based approach, simple geometric primitives (points, lines, curves, *etc.*), called the image features, are used to 'abstract' the images [9]. They can be either detected automatically, or marked by hand. A geometric distance between such features is eventually minimized.

The other approach is called pixel-based (or direct approach). It consists in minimizing the discrepancy between the color of the pixels matched by the warp [1].

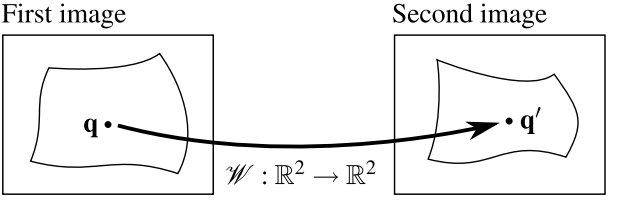

Figure 1: A warp $\mathscr{W}$ is a function that maps a 2D point $\mathbf{q}$ from the first image to a point $\mathbf{q}'$ in the second image.

In this paper, we bring several contributions. We first demonstrate in section 2 that the classical BS-Warp corresponds to affine imaging condition, in the sense that it models the affine projection of some 3D surface. We then propose our most important contribution in section 3: a novel parametric warp we call *NURBS-Warp*, that extends the classical BS-Warp to perspective projection. This warp has a simple analytical form: it is obtained as the two-way tensor-product of bivalued Non-Uniform Rational B-Splines (NURBS). Finally, we give in section 4 algorithms for the feature-based estimation of our NURBS-Warp. More precisely, we consider that a set $\{\mathbf{q}_k \leftrightarrow \mathbf{q}'_k\}_{k=1,\dots,r}$ of point correspondences between the two images is known, and show how the parameters that minimize the classical *transfer error* can be found, by solving:

$$\min_{\mathbf{x}} \sum_{k=1}^{r} d^2\left(\mathbf{q}'_k, \mathscr{W}(\mathbf{q}_k;\mathbf{x})\right), \tag{1}$$

where $\mathscr{W}$ represents the warp and $d^2(\mathbf{a},\mathbf{b})$ is the squared euclidean distance between the points $\mathbf{a}$ and $\mathbf{b}$. We finally report experimental results in section 5 and conclude the paper.

2 BS-Warps

Definition. We denote $\mathscr{W}_B$ the BS-Warp. Following the literature about B-Splines (for instance, [6, 7]), the BS-Warp can be defined as the tensor-product of monodimensional B-Splines:

$$\mathscr{W}_B(\mathbf{q};\mathbf{x}) = \sum_{i=1}^{m}\sum_{j=1}^{n} \mathbf{p}_{ij} N_i(x) N_j(y), \tag{2}$$

where the functions $N_i : \mathbb{R} \rightarrow \mathbb{R}$ are the B-Spline basis functions of degree three[1] and the $\mathbf{p}_{ij} = (p^x_{ij}, p^y_{ij})^\mathsf{T}$ are the control points (grouped in the parameter vector $\mathbf{x} \in \mathbb{R}^{2mn}$). The scalars m and n are the number of control points along the x and y directions respectively. Note that we consider as coincident the knot sequences used to define the B-Spline basis functions.

Affine interpretation. If we consider that the observed surface is modeled by a threedimensional tensor-product B-Spline, the BS-Warp corresponds to the transformation between the two images under affine imaging conditions (see figure 2 for an illustration).

[1] A B-Spline can actually be of any degree but we restrict our study to degree 3 since it is a good compromise between flexibility and efficiency.

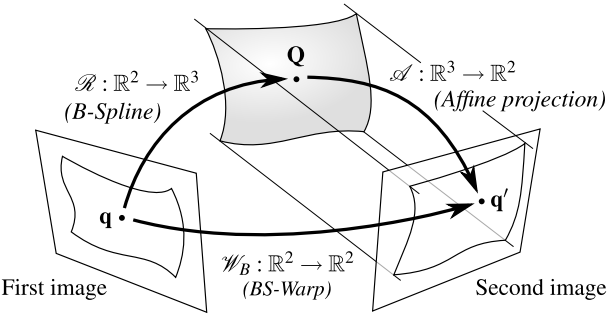

Figure 2: A BS-Warp can be seen as the result of a threedimensional B-Spline surface projected under affine conditions.

Let $\mathscr{R} : \mathbb{R}^2 \rightarrow \mathbb{R}^3$ be the 2D-3D map between the first image and the threedimensional surface:

$$\mathbf{Q} = \mathscr{R}(\mathbf{q};\mathbf{x}) = \sum_{i=1}^{m}\sum_{j=1}^{n} \bar{\mathbf{p}}_{i,j} N_i(x) N_j(y), \tag{3}$$

with $\bar{\mathbf{p}}_{i,j} = (\bar{p}^x_{i,j}\, \bar{p}^y_{i,j}\, \bar{p}^z_{i,j})^\mathsf{T} \in \mathbb{R}^3$ the 3D control points of the surface. Let $\mathscr{A} : \mathbb{R}^3 \rightarrow \mathbb{R}^2$ be the affine projection of the surface into the second image:

$$\mathscr{A}(\mathbf{Q}) = \mathsf{A}\mathbf{Q}, \tag{4}$$

with A the matrix which models the affine projection, assuming that the 3D surface is expressed within the coordinate frame of the second camera:

$$\mathsf{A} = \begin{pmatrix} a_x & 0 & 0 \\ 0 & a_y & 0 \end{pmatrix}. \tag{5}$$

Given these notations, the warped point $\mathbf{q}'$ can be written $\mathscr{A}(\mathscr{R}(\mathbf{q}))$ which, after expansion, gives:

$$\mathbf{q}' = \sum_{i=1}^{m}\sum_{j=1}^{n} \begin{pmatrix} \bar{p}^x_{i,j} \\ \bar{p}^y_{i,j} \end{pmatrix} N_i(x) N_j(y). \tag{6}$$

Equation (6) matches the definition (2) of a BS-Warp. □

BS-Warps are not suited for perspective imaging conditions. As we just demonstrated, BS-Warps are obtained under affine imaging conditions. In this paragraph, we illustrate that BS-Warps are indeed not suited for perspective imaging conditions. This comes from the fact that the division appearing in a perspective projection is not present in the BS-Warp model.

The bad behavior of the BS-Warp in the presence of perspective effects is illustrated in figure 3. In this experiment, we simulate a set of point correspondences by transforming a regular grid with an homography parameterized by a scalar a that controls the amount of perspective effect. The 3×3 matrix of this homography, H_a, is given by:

$$\mathsf{H}_a \propto \frac{1}{a} \begin{pmatrix} (a+1)^2/4 & 0 & -(a^2-1)/4 \\ 0 & a(a+1)/2 & 0 \\ -(a^2-1)/4 & 0 & (a+1)^2/4 \end{pmatrix}, \tag{7}$$

where $\propto$ indicates equality up to scale. The larger $|a-1|$, the more important the perspective effect. Figure 3c clearly shows that the transformation can be correctly modeled by a BS-Warp only when $a = 1$, *i.e.* when the perspective effect is almost inexistant. Figure 3d shows that the number of control points of a BS-Warp must be significantly large in order to correctly model a perspective effect.

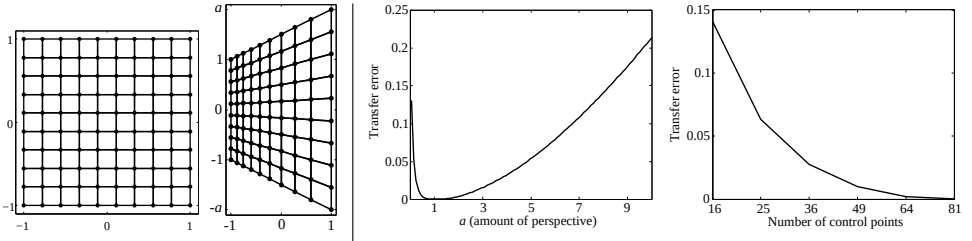

(a) (b) (c) (d)

Figure 3: Bad behavior of the BS-Warp in the presence of perspective effects. (a) Data points on a regular grid (first image). (b) Transformed points simulating a perspective effect with an homography (second image). (c) Influence of the perspective effect on a BS-Warp with 16 control points. (d) The perspective effect ($a = \frac{5}{2}$) can be modeled with a BS-Warp but it requires a large amount of control points.

3 NURBS-Warps

This section introduces a new warp, the NURBS-Warp, which is built upon tensor-product Non-Uniform Cubic B-Splines. We show that the NURBS-Warp naturally appears when replacing the affine projection by a perspective one in the image formation model of the previous section. As our experimental results show, the NURBS-Warp performs better in the presence of perspective effects.

Perspective interpretation. Following the same reasoning as for the BS-Warp in the previous section, we show that the NURBS-Warp corresponds to perspective imaging conditions. This is illustrated in figure 4.

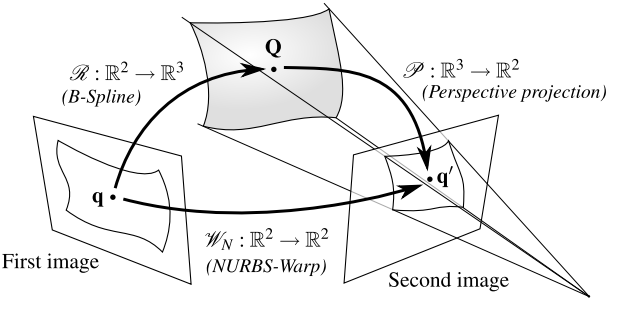

Figure 4: A NURBS-Warp can be seen as the result of a threedimensional B-Spline surface projected under perspective conditions.

Let $\mathscr{P}$ be the perspective projection:

$$\mathscr{P}(\mathbf{Q}) = \psi(\mathsf{K}\mathbf{Q}), \tag{8}$$

with K the matrix of intrinsic parameters for the second camera. ψ is the homogeneous to affine coordinates function, *i.e.* $\psi(\check{\mathbf{q}}) = \mathbf{q}$ where $\check{\mathbf{q}}$ are the homogeneous coordinates of $\mathbf{q}$ ($\check{\mathbf{q}}^\mathsf{T} = (\mathbf{q}^\mathsf{T}\ 1)$). We assume that the image coordinates are chosen such that the origin coincides with the principal point:

$$\mathsf{K} = \begin{pmatrix} f_x & 0 & 0 \\ 0 & f_y & 0 \\ 0 & 0 & 1 \end{pmatrix}. \tag{9}$$

Replacing $\mathbf{Q}$ by its expression (3) in equation (8) leads to:

$$\mathscr{P}(\mathbf{Q}) = \mathscr{P}(\mathscr{R}(\mathbf{q})) = \frac{1}{\sum_{i=1}^{m}\sum_{j=1}^{n} \bar{p}^z_{i,j} N_i(x) N_j(y)} \begin{pmatrix} f_x \sum_{i=1}^{m}\sum_{j=1}^{n} \bar{p}^x_{i,j} N_i(x) N_j(y) \\ f_y \sum_{i=1}^{m}\sum_{j=1}^{n} \bar{p}^y_{i,j} N_i(x) N_j(y) \end{pmatrix}. \tag{10}$$

Defining $w_{i,j} = \bar{p}^z_{i,j}$, $p^x_{i,j} = f_x \frac{\bar{p}^x_{i,j}}{w_{i,j}}$ and $p^y_{i,j} = f_y \frac{\bar{p}^y_{i,j}}{w_{i,j}}$, equation (10) is the very definition of a tensor-product NURBS [5] with control points $\mathbf{p}^\mathsf{T}_{i,j} = (p^x_{i,j}, p^y_{i,j})$ and weights $w_{i,j}$. We denote $\mathscr{W}_N$ this new warp and call it a *NURBS-Warp*:

$$\mathscr{W}_N(\mathbf{q};\mathbf{x}) = \frac{\sum_{i=1}^{m}\sum_{j=1}^{n} \mathbf{p}_{i,j} w_{i,j} N_i(x) N_j(y)}{\sum_{i=1}^{m}\sum_{j=1}^{n} w_{i,j} N_i(x) N_j(y)}. \tag{11}$$

Here, the warp parameters, *i.e.* the control points and the weights, are grouped into a vector $\mathbf{x} \in \mathbb{R}^{3mn}$.

Using the NURBS-Warp in the setup used for the experiment of figure 3 leads to a transfer error consistently smaller than 10^{-5} pixels.

Homogeneous NURBS-Warp. The NURBS-Warp defined by equation (11) can be expressed with homogeneous coordinates. We note $\check{\mathscr{W}}_N$ the NURBS-Warp in homogeneous coordinates:

$$\check{\mathscr{W}}_N(\mathbf{q};\mathbf{x}) \propto \begin{pmatrix} \frac{\sum_{i=1}^{m}\sum_{j=1}^{n} p^x_{i,j} w_{i,j} N_i(x) N_j(y)}{\sum_{i=1}^{m}\sum_{j=1}^{n} w_{i,j} N_i(x) N_j(y)} \\ \frac{\sum_{i=1}^{m}\sum_{j=1}^{n} p^y_{i,j} w_{i,j} N_i(x) N_j(y)}{\sum_{i=1}^{m}\sum_{j=1}^{n} w_{i,j} N_i(x) N_j(y)} \\ 1 \end{pmatrix} \propto \sum_{i=1}^{m}\sum_{j=1}^{n} \begin{pmatrix} p^x_{i,j} w_{i,j} \\ p^y_{i,j} w_{i,j} \\ w_{i,j} \end{pmatrix} N_i(x) N_j(y). \tag{12}$$

We observe that in the homogeneous version of equation (12), our NURBS-Warp does a linear combination of control points in homogeneous coordinates, as opposed to the classical BS-Warp of equation (2) that does a linear combination of control points in affine coordinates. This is what makes our NURBS-Warp able to model perspective projection, thanks to the division 'hidden' in the homogeneous coordinates.

4 Parameter Estimation

In this section, we show how the BS-Warp and the NURBS-Warp parameters can be estimated, *i.e.* how the following minimization problem can be solved:

$$\min_{\mathbf{x}} \sum_{k=1}^{r} d^2\left(\mathbf{q}'_k, \mathscr{W}(\mathbf{q}_k;\mathbf{x})\right). \tag{13}$$

4.1 The BS-Warp

The dependency of the BS-Warp to its parameters is linear. As a consequence, the optimization problem (13) for a BS-Warp simply reduces to an ordinary linear least-squares minimization problem.

4.2 The NURBS-Warp

Contrarily to the BS-Warp, the dependency of the NURBS-Warp to its parameters is not linear. Problem (13) thus leads one to a non-linear least-squares optimization problem. It is a well-known fact that this kind of problem can be efficiently solved using an iterative algorithm such as Levenberg-Marquardt. Such an algorithm needs an initial solution. We propose three approaches to compute an initial set of parameters (which are further detailed in the sequel of this section):

- **First approach:** Act as if the images were taken under affine imaging conditions.
- **Second approach:** Act as if the warp relating the two images was an homography.
- **Third approach:** Use an algebraic approximation to the transfer error function.

Since all of these three approaches are relatively cheap to compute, it is possible to test the three of them and choose as initial parameters those that give the smallest transfer error.

First approach (affine initialization). An initial solution for the NURBS-Warp estimation problem can be computed by setting all the weights to 1. By doing so, the equation defining a NURBS-warp reduces to the expression of a simple BS-Warp. An initial set of parameters can thus be computed using ordinary least-squares minimization. Since the BS-Warp corresponds to affine imaging conditions, this approach is expected to give good results when the effects of perspective are limited.

Second approach (homographic warp). Even if the homographic warp is not suited to deformable environments, it can be a good approximation (particularly if the surface bending is not important). We denote $\mathscr{W}_H$ the homographic warp. It is defined by:

$$\mathscr{W}_H(\mathbf{q};\mathbf{x}) = \frac{1}{p_7x + p_8y + 1}\begin{pmatrix} p_1x + p_2y + p_3 \\ p_4x + p_5y + p_6 \end{pmatrix}, \tag{14}$$

with $\mathbf{x}^\mathsf{T} = (p_1 \ \dots \ p_8)$. Minimizing the transfer error of equation (13) with the homographic warp $\mathscr{W}_H$ can be achieved iteratively using, for instance, the Levenberg-Marquardt algorithm (and by taking the identity warp or the algebraic solution as an initialization). A complete review of homographic warp estimation can be found in [8].

Third approach (algebraic approximation). The third and last approach we propose to initialize the optimization process consists in minimizing an algebraic approximation to the transfer error:

$$\min_{\mathbf{x}} \sum_{k=1}^{r} d_a^2\left(\mathbf{q}'_k, \check{\mathscr{W}}_N(\mathbf{q}_k;\mathbf{x})\right), \tag{15}$$

with $d_a^2(\mathbf{q}', \check{\mathbf{q}}) = \|\mathsf{S}(\tilde{\mathbf{q}}' \times \check{\mathbf{q}})\|^2$ an algebraic distance between the points[2] $\mathbf{q}$ and $\mathbf{q}'$. The operator S removes the last element of a 3-vector. $\tilde{\mathbf{q}}'$ are the scaled homogeneous coordinates of $\mathbf{q}'$ (*i.e.* $\tilde{\mathbf{q}}'^{\mathsf{T}} = (\mathbf{q}'^{\mathsf{T}}\ 1)$). If we make the following variable change in expression (12) of the homogeneous NURBS-Warp: $a_{i,j} = p^x_{i,j} w_{i,j}$ and $b_{i,j} = p^y_{i,j} w_{i,j}$ then it is straightforward to see that the algebraic distance is the squared euclidean norm of an expression linear with respect to the parameters $a_{i,j}$, $b_{i,j}$ and $w_{i,j}$. Replacing the algebraic distance by its expression in the initial optimization problem of equation (15) leads to homogeneous linear least-squares. This problem can be solved with singular value decomposition [3].

5 Experiments

5.1 Simulated Data

Simulation setup. We generate two images by simulating two cameras looking at a surface with different deformations between the views. The surface is generated as a linear combination of two objects: a simple plane and a more deformed surface (see figure 5). A single parameter, α, controls the amount of surface bending. Points on the surface are projected on the images and corrupted with an additive gaussian noise. The perspective effect is controlled by varying the distance between the scene and the camera (the focal length, f, is adjusted so that the apparent size of the imaged surface remains approximately the same). The influence of three quantities are tested independently:

- the amount of noise: controlled by the standard deviation σ in pixels;
- the amount of bending: controlled by the previously described parameter α;
- the amount of perspective: controlled by the scene to camera distance d, in pixels.

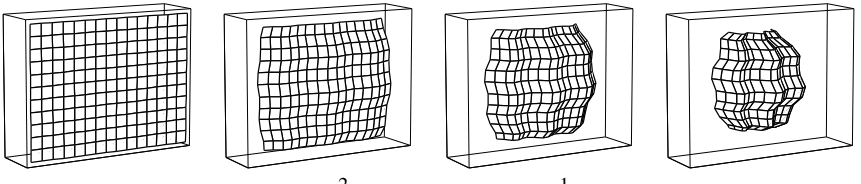

$\alpha = 1$ $\alpha = \frac{2}{3}$ $\alpha = \frac{1}{3}$ $\alpha = 0$

Figure 5: The simulated threedimensional surfaces used in our experiments are obtained as linear combinations of a plane ($\alpha = 1$) and of a more distorted surface ($\alpha = 0$).

The default simulation parameters are $r = 192$ point correspondences, $\sigma = 1$ pixel, $\alpha = \frac{1}{2}$, $d = 800$ pixels, $f = 400$ pixels and n control points. These parameters yield mild perspective effects. For each set of parameters, the generated surface is also rotated around its center. The reported results are the average of the mean transfer error over 100 surfaces which have different rotations and corruptions of the projected points. For each varied parameter, three plots report the results for different numbers of control points ($n = 16$, $n = 25$ and $n = 36$). Four curves are reported on each plot. They correspond to the homographic warp, the initial estimate of the NURBS-Warp using the algebraic distance, the optimal BS-Warp and the final NURBS-Warp.

[2] This algebraic distance is valid only if the point coordinates are normalized according to [8]. We did not introduced it in our equations for the sake of clarity.

Two general observations can be made about those results. First, the experiments show that the NURBS-Warp always outperforms the three other approaches. This comes from the fact that it is designed, by construction, to model more complex deformations between images[3]. Second, the following results show that the larger the number of control points, the lower the transfer error.

Influence of noise. Figure 6 shows the influence of the amount of noise on the estimated warps. We can see that the influence of this factor is relatively limited and, more importantly, that this influence is similar for all the four warps.

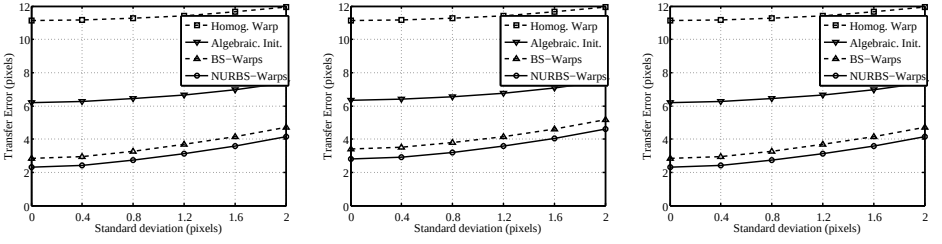

$n = 16$ control points $n = 25$ control points $n = 36$ control points

Figure 6: The influence of the amount of noise.

Influence of bending. The influence of the amount of bending is studied by varying the parameter α. The results are reported in figure 7. This experiment shows, as expected, that the homographic warp is the one which is the most influenced by the deformations of the observed surface. It comes from the fact that the homographic warp inherently does not model deformable environments.

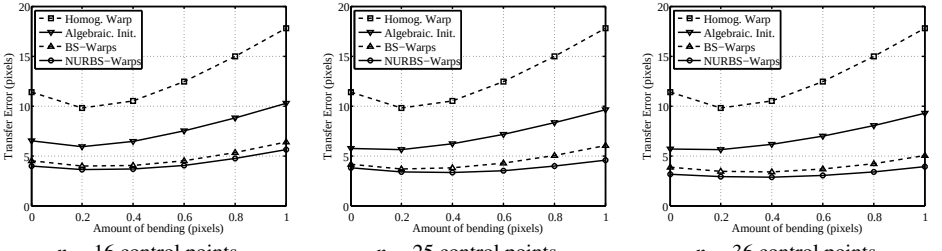

$n = 16$ control points $n = 25$ control points $n = 36$ control points

Figure 7: The influence of the amount of bending.

Influence of perspective (1). The influence of the perspective effect is studied by varying the scene to camera distance: the larger the distance, the more affine the imaging conditions. The results are reported in figure 8. This experiment truly reveals the full power of the proposed NURBS-Warp. Indeed, for the lowest number of control points ($n = 16$), we see that with an important perspective effect ($d = 270$), the NURBS-Warp is more than twice as good as the BS-Warp. Two main reasons explain this result. First, the NURBS-Warp has

[3] Besides, it seems natural that the NURBS-Warp estimate is better than the other approaches since its parameter estimation starts from an initial solution which corresponds to the parameters of the best estimate among the three other approaches.

been designed to model perspective effects. Second, the behavior of the BS-Warp is better for affine imaging conditions. Figure 8 also shows that the BS-Warp can correctly model the deformations but it requires a large amount of control points.

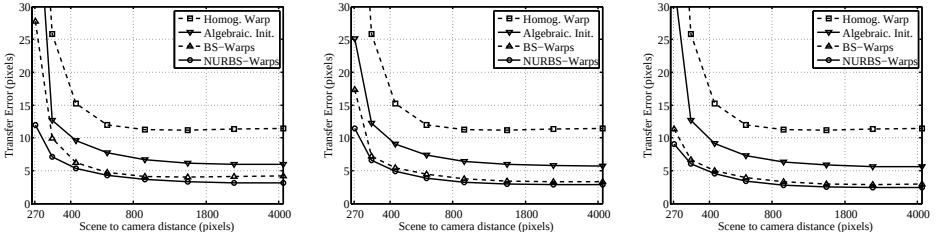

$n = 16$ control points $n = 25$ control points $n = 36$ control points

Figure 8: The influence of the amount of perspective.

Influence of perspective (2). In the previous experiment the warps had to cope simultaneously with perspective effects and large surface deformations. As a consequence, it is difficult to see the benefit brought by our NURBS-Warp. We thus present the influence of perspective with less complex deformations. We use the same experimental setup except for the generated surface which is now obtained as the linear combination of a plane and a half-cylinder (see figure 9a). Figure 9c shows that the NURBS-Warp brings a real benefit compared to the BS-Warp when the perspective effect are important: for example, we see that compared to the BS-Warp, the NURBS-Warp transfer error is over 3 times lower for a camera to scene distance of 270 pixels.

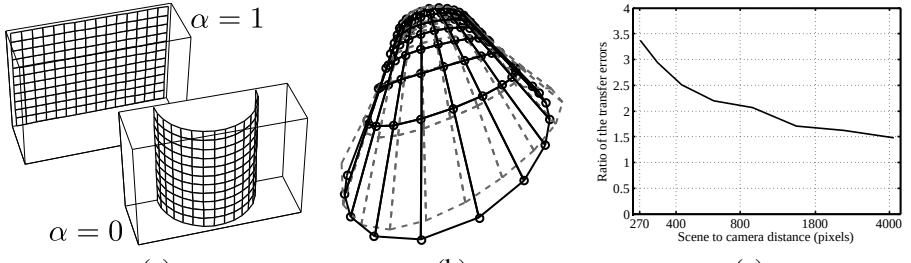

(a) (b) (c)

Figure 9: (a) Simple deformations are obtained using a linear combination of a plane and a half-cylinder. (b) The NURBS-Warp (black visualization grid) models better the perpective effect than the BS-Warp (dashed grid). The black circles represent the ground truth location of the vertices. (c) The BS-Warp transfer error divided by the one of the NURBS-Warp.

From the last two experiments, we can say that the proposed NURBS-Warp is well suited for large perspective effects. However, when the surface deformations are significant, both the NURBS-Warp and the BS-Warp require a lot of control points. Since it increases the number of degree of freedom, the BS-Warp can also cope with perspective effects.

5.2 Real Images

Figures 10 and 11 show examples of warps estimated for a rigid and a deformable scene respectively. The warps are estimated from 130 point correspondences that we entered man-

ually (represented by the small circles). We set the number of control points to 16 for both the BS-Warp and the NURBS-Warp. The estimated warps are represented by a visualization grid. This grid is shown in its rest position in the first image. It is then transferred into the second image using the estimated warps. The conclusion of this experiment is that the NURBS-Warp is the one that gives the best results. This is especially true when perspective effects and surface deformations are combined. In particular, we can see in figure 11 that the NURBS-Warp is the only warp able to retrieve realistic surface deformations.

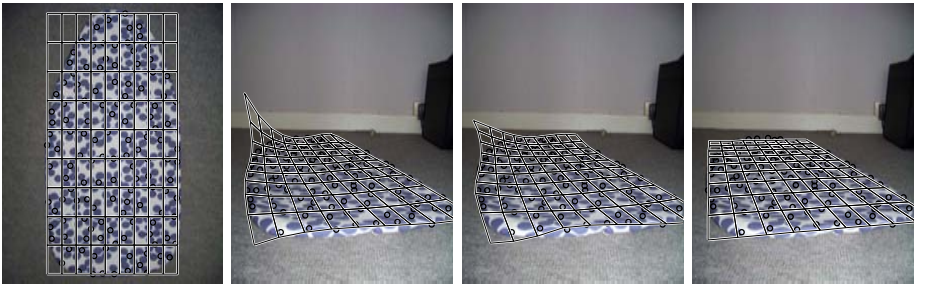

First image | TE=9.2 BS-Warp | TE=7.8 NURBS-Warp | TE=14.5 Homography

Figure 10: Warp estimated for a rigid surface (TE: Transfer Error in pixels).

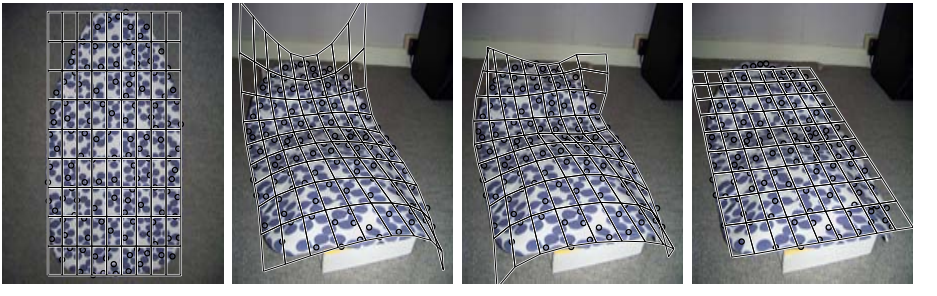

First image | TE=21.2 BS-Warp | TE=12.6 NURBS-Warp | TE=52.3 Homography

Figure 11: Warp estimated for a deformable scene (TE: Transfer Error in pixels).

6 Conclusion

We introduced a new parametric warp we called NURBS-Warp. It was derived by analyzing the classical BS-Warp, that we showed is based on the two-way tensor product of bivariate B-Splines. As a first contribution, we showed that the BS-Warp is intrinsically affine: it does not model the effect of perspective projection. Our NURBS-Warp, based on the tensor product of NURBS, is an extension of the BS-Warp. It models perspective projection, and thus copes with more complex deformations with less control points, as our experimental results show. An estimation procedure from point correspondences was given. It allowed us to demonstrate the representational power of our warp compared to the BS-Warp, and against various factors such as noise, surface shape and number of control points. However, it might be interesting for future work to study how classical robust and pixel-based methods can be applied to our NURBS-Warp.

References

[1] A. Bartoli and A. Zisserman. Direct estimation of non-rigid registrations. In *Proceedings of the British Machine Vision Conference*, 2004.

[2] A. Bartoli, M. Perriollat, and S. Chambon. Generalized Thin-Plate Spline warps. In *Proceedings of the Conference on Computer Vision and Pattern Recognition*, 2007.

[3] Å. Björck. *Numerical Methods for Least Squares Problems*. SIAM, Philadelphia, Penn., 1996.

[4] F. L. Bookstein. Principal warps: Thin-Plate Splines and the decomposition of deformations. *IEEE Transactions on Pattern Analysis and Machine Intelligence*, 11(6): 567–585, June 1989.

[5] N. Carlson. NURBS surface fitting with Gauss-Newton. Master's thesis, Luleå University of Technology, 2009.

[6] C. de Boor. *A Practical Guide to Splines – Revised Edition*. Springer, 2001.

[7] P. Dierckx. *Curve and surface fitting with splines*. Oxford University Press, Inc., 1993.

[8] R. Hartley and A. Zisserman. *Multiple View Geometry in Computer Vision, Second Edition*. Cambridge University Press, 2003.

[9] J. Pilet, V. Lepetit, and P. Fua. Fast non-rigid surface detection, registration and realistic augmentation. *International Journal of Computer Vision*, 76(2):109–122, February 2008.

[10] D. Rueckert, L. I. Sonoda, C. Hayes, D. L. G. Hill, M. O. Leach, and D. J. Hawkes. Nonrigid registation using Free-Form Deformations: Application to breast MR images. *IEEE Transactions on Medical Imaging*, 18(8):712–721, August 1999.